Journal of Alloys and Compounds 506 (2010) 423–427

Contents lists available at ScienceDirect

Journal of Alloys and Compounds

journal homepage: www.elsevier.com/locate/jallcom

Pore structure and mechanical properties in freeze cast porous Si_3N_4 composites using polyacrylamide as an addition agent

Feng Ye*, Jingyi Zhang, Haijiao Zhang, Limeng Liu

School of Materials Science and Engineering, Harbin Institute of Technology, Harbin 150001, PR China

ARTICLE INFO

Article history:
Received 15 April 2010
Received in revised form 30 June 2010
Accepted 6 July 2010
Available online 14 July 2010

Keywords:
Porous Si_3N_4 ceramics
Polyacrylamide
Freeze casting
Microstructure
Mechanical properties

ABSTRACT

Porous barium aluminosilicate (BAS)/Si_3N_4 composites were prepared by freeze casting process using liquid N_2 as refrigerant. The pore morphologies, $\alpha \rightarrow \beta$-Si_3N_4 phase transformation, and mechanical properties of the resultant porous ceramics were strongly affected by the addition of polyacrylamide (PAM) into the slurries. The incorporation of 2 wt.%PAM changed the ice crystals structure from lamellar with dendrites into featureless columnar ones, the feature of which was duplicated by the pores in the sintered ceramics. The lamellar pores with dendrites could favor the $\alpha \rightarrow \beta$-Si_3N_4 phase transformation, but were detrimental to the mechanical properties. The sample with 1 wt.%PAM exhibited the highest strength and toughness in the resultant porous composites due to its columnar pore structure with less dendritic pores and higher aspect ratio of β-Si_3N_4 grains. A relative dense layer was formed at the bottom of the samples with PAM and its thickness increased with increasing PAM content.

1. Introduction

Advanced porous ceramics with high porosity and large surface area were widely used as filters, bio-prosthetic implants, catalyst supports and lightweight structural materials [1,2]. Porous silicon nitride is a promising candidate owing to their excellent mechanical and thermal–mechanical properties [3,4]. A number of manufacturing techniques, namely adding fugitive substance [5], partial sintering by using less sintering aid [6,7], partial hot-pressing [8] have been developed for the production of porous silicon nitride ceramics.

Recently, the freeze casting process has been developed to produce highly porous ceramics, because it can produce interconnected pore channels in a controllable manner, which offers superior mechanical properties and functions [9]. Freeze casting has already been used for fabricating a wide variety of ceramic materials [10–13]. However, till now, the reports on the microstructural control and mechanical properties of porous silicon nitride ceramics fabricated by freeze casting are very scarce. Polyacrylamide (PAM) is a water soluble polymer of acrylamide monomers. It can be used in a variety of industries including food, water treatment and agricultural industries. Barium aluminosilicate (BAS) has been proved to be an excellent sintering additive to promote the α- to β-Si_3N_4 transformation and the growth of elongated β-Si_3N_4 grains [14]. The current work is concerned with the microstructure control of porous BAS/Si_3N_4 composites by changing the PAM content.

2. Experimental procedures

The materials used in this study were BAS/Si_3N_4 composites with 10 wt.%BAS. Starting materials were Si_3N_4 (supplied by Shanghai Junyu Ceramic Co., Ltd., China, α-Si_3N_4 content >95%, average particle size is 0.5–1.0 μm) and BAS glass–ceramic. The BAS glass–ceramic powder was synthesized through the hydrolysis of alkoxides [15]. First, BAS and Si_3N_4 powders were well dispersed in the distilled water with 0.3 wt.% polyacrylic acid (PAA) (based on powders) as dispersant and different amount of PAM (Shanghai Chemical Reagent Corp., China), and then ball-milled for 20 h to obtain stable slurries. In order to investigate the effect of PAM concentration on the microstructure of the samples, the solid loadings of the slurries were fixed to 40 vol.% and 0, 1 and 2 wt.%PAM (based on water) were dissolved in the water.

The prepared slurries were then poured into polyethylene molds (ϕ70 mm × 15 mm) using a brass bottom plate immersed in liquid N_2. The top of the container was open so that the upper surface of the slurry would expose to the atmosphere at room temperature. Immediately after casting, the ice crystals grow unidirectionally from the bottom to the upper surface of the slurry. After the frozen BAS/Si_3N_4 samples were completely freeze-dried under vacuum for 2 days, they were carefully placed into a graphite crucible with a silicon nitride-based powder bed and sintered in a graphite resistance furnace at 1800 °C for 2 h under a 0.1 MPa nitrogen atmosphere. The heating and cooling rates were both 5 °C/min.

The densities of the samples were calculated from the dimensions and weight of the samples. Pore size distribution was measured by mercury porosimetry (Model Autopore III 9420, Micrometics Co., USA).

Flexural strength and fracture toughness were measured in air at room temperature. All flexural bars were machined with the tensile surface perpendicular to the freezing direction. Flexural strength measurements were performed on bar specimens (3 mm × 4 mm × 36 mm) using a three-point bend fixture with a span of 30 mm. Fracture toughness measurements were performed on single-edge-notch beam specimens (2 mm × 4 mm × 30 mm) with a span of 16 mm, and a half-thickness notch was made using a 0.1 mm thick diamond wafering blade. At least, six specimens were tested for each test condition.

* Corresponding author. Tel.: +86 45186413921; fax: +86 45186413922.
E-mail address: yf306@hit.edu.cn (F. Ye).

0925-8388/$ – see front matter © 2010 Elsevier B.V. All rights reserved.
doi:10.1016/j.jallcom.2010.07.020

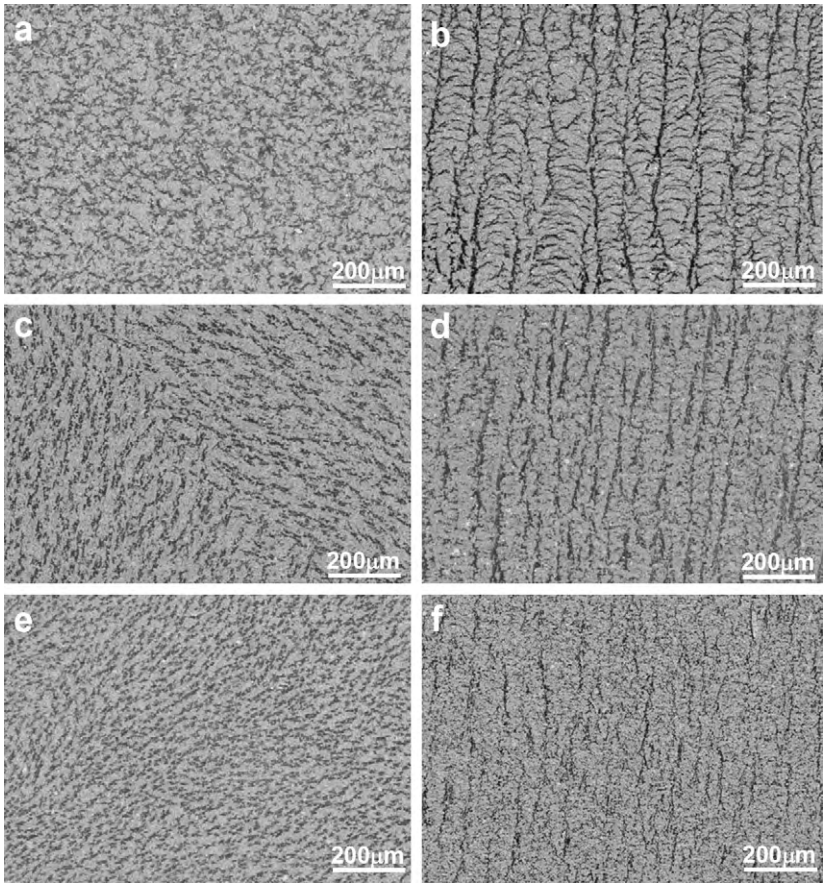

Fig. 1. Back scattered electron mode SEM micrographs of the porous Si_3N_4 ceramics perpendicular to (a, c and e) and parallel to the ice growth direction (b, d and f): (a and b) 0 wt.%PAM; (c and d) 1 wt.%PAM; (e and f) 2 wt.%PAM.

Crystalline phases of the sintered Si_3N_4/BAS composites were characterized by X-ray diffraction (XRD). Quantitative analysis of α- and β-Si_3N_4 phase content was determined by comparing the peak intensity ratios [16]. The microstructure of porous Si_3N_4 samples was characterized by scanning electron microscopy (SEM; Model JSM-5600, JEOL Ltd., Tokyo, Japan). In order to evaluate the pore structure, the obtained porous Si_3N_4 ceramics were also infiltrated with an epoxy resin and analyzed by SEM using backscattered electron mode (BSE).

3. Results and discussion

Fig. 1 shows the typical pore structures of the obtained porous BAS/Si_3N_4 composites with the different PAM concentrations from 0 to 2 wt.%. With the increase in the amount of PAM, the pore size decreased and the pore structure changed from the lamellar pores with dendrites (Fig. 1b) to columnar ones without dendritic pores.

In freeze casting, the pore structure is a replica of the morphology of the ice crystal. During the solidification of the suspension, a liquid film should exist between the ice front and the particle, which acts as the transmission medium of water molecules for the ice growth [13]. Fig. 2 demonstrates that a particle with radius r is moving ahead of a solid–liquid interface advanced with a velocity of υ. A particle is either engulfed or ejected by the ice fronts depends on the two competitive forces acting on the suspended particles [17], i.e. the attractive force (F_η) and the repulsive force (F_σ). The attractive force resulted from viscous drag would push the particles to the solid and favor entrapment. It can be given by the following equation [18]:

$$F_\eta = \frac{6\pi\eta\upsilon r^2}{d} \quad (1)$$

where η is the solution viscosity, r is the particle radius, d is the distance between particle and solid–liquid interface and υ is the velocity of the solidification front.

The repulsive force would hinder particle engulfment, which is caused by the different interfacial free energy among solid-particle (σ_{sp}), liquid-particle (σ_{lp}) and solid–liquid (σ_{sl}) interface and can be defined in Eq. (2) [19]:

$$F_\sigma = 2\pi r\Delta\sigma_0\left(\frac{a_0}{d}\right)^n \quad (2)$$

$$\Delta\sigma_0 = \sigma_{sp} - (\sigma_{sl} + \sigma_{lp}) \quad (3)$$

where a_0 is the average intermolecular distance in the film, n is an exponent and $\Delta\sigma_0$ is the balance of the surface free energies at the solid/solution/particle boundary. When $F_\eta \geq F_\sigma$, the particles will be pushed to the solid–liquid interface, and then the distance of the

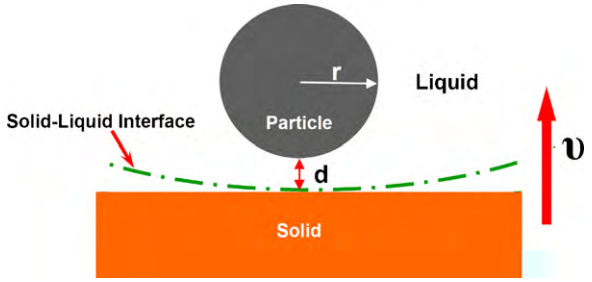

Fig. 2. Schematic of a moving particle of radius r ahead of a solid–liquid interface during freeze casting of ceramic slurries. d is the distance between particle and solid–liquid interface and υ is the velocity of the advancing solidification front.

Table 1
Properties of the porous Si_3N_4 ceramics with varied PAM concentration.

Material	$\beta/(\alpha+\beta)$ (%)	Porosity[a] (%)	Porosity[b] (%)	Flexural strength (MPa)	Fracture toughness (MPam$^{1/2}$)
0 wt.%PAM	77.3	38.0 ± 1	36.6 ± 1	57 ± 6	1.5 ± 0.1
1 wt.%PAM	56.5	42.4 ± 1	40.7 ± 2	111 ± 7	1.8 ± 0.1
2 wt.%PAM	38.9	44.8 ± 2	42.0 ± 2	75 ± 9	1.6 ± 0.2

[a] Calculated from the sample dimension and weight.
[b] Measured by mercury porosimetry.

gap may be not sufficient to keep the ice crystal surface growing and hence resulting in the particle engulfment.

In the obtained porous composites, the main parallel channels from the bottom to the upper surface of the slurry were formed in all three samples, indicating that the particles are ejected by the main ice front owing to $F_\sigma \geq F_\eta$. During the growth of the ice crystals, the ceramic particles together with PAM were expelled from the freezing front and thus increasing the solute concentration around the existed main ice crystals, which would increase the attractive force of F_η due to the increased solution viscosity. Incorporation of high amount of PAM could further increase the solution viscosity and the attractive force, which eventually would result that the attractive force exceeds the repulsive force. Therefore, the corresponding liquid film (between the ice front and the particle) thickness in the sample with a high PAM content would not be enough to allow the necessary flow of molecules to keep the crystal growing and hence preventing the branch ice crystals growing from the main ice crystals.

The porosities analyzed by mercury porosimetry were almost the same as those calculated from the dimensions and weights of the samples, as shown in Table 1. It reveals that most of the pores in the resultant porous composites are open. The effect of the PAM content on the pore size distribution is shown in Fig. 3. All the three samples exhibit a bimodal pore size distribution. The small pores below 1 μm correspond to the pores formed by the branch ice crystals and the big ones above 1 μm around to the main channels. With increasing the PAM content from 0 to 2 wt.%, the peak below 1 μm tends to disappear, which is due to the disappearance of branch ice crystals.

It is known that the increase in ice crystal size is caused mainly by Ostwald ripening. Ostwald ripening is a well-known phenomenon in which the larger crystals increase in size at the expense of the smaller crystals. In this study, Ostwald ripening is restricted by the mass transport of water. The concentrated solution decreases the mass transfer coefficient of water molecules, thus retard the growth of ice crystals. So when PAM was added to the suspension, small ice crystal was obtained and thus decreasing the pore size, as shown in Fig. 1. The ice front velocity parallel to the crystallographic c axis (the direction perpendicular to the lamellar ice crystals corresponds to the limited growth direction of ice crystals) is 10^2–10^3 times lower than the velocity perpendicular to this axis [20], so as the PAM content increased, the reduction of ice crystal size in the direction of perpendicular to c axis is more evident than parallel to c axis direction, and the pore morphology change from lamellar to columnar.

Fig. 4 shows the cross-sectional SEM micrographs of the obtained porous Si_3N_4 composites, indicating *in situ* formation of a dense layer at the bottom of the samples with PAM (Fig. 4b and c). During freeze casting, initial freezing is very fast and then the velocity of the liquid front decreases rapidly until it reaches a steady state with an approximate constant value. Consequently, the ceramic

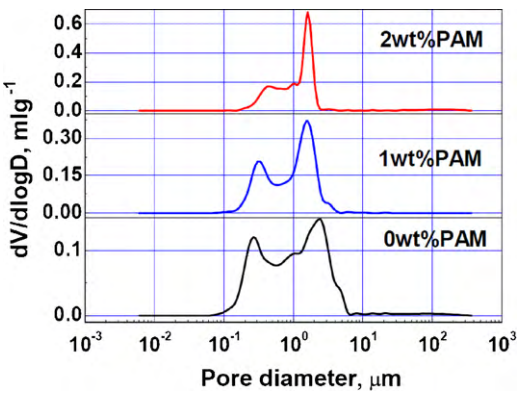

Fig. 3. Pore size distribution of porous Si_3N_4 ceramics with different PAM contents.

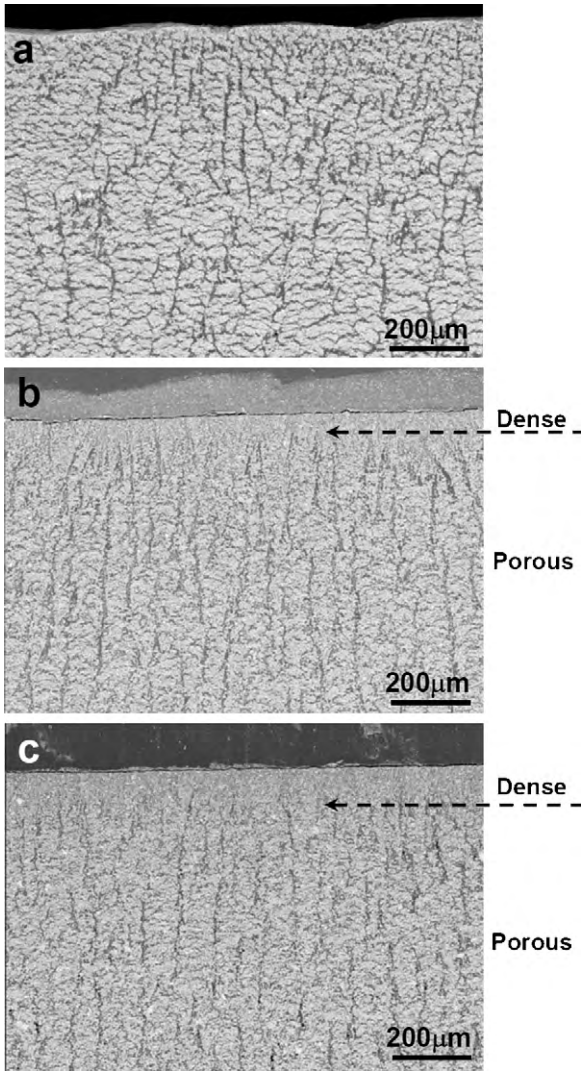

Fig. 4. Cross-sectional SEM micrographs of the obtained porous Si_3N_4 composites, showing the *in situ* formation of a dense layer at the bottom of the samples with PAM: (a) 0 wt.% PAM; (b) 1 wt.%PAM; (c) 2 wt.%PAM.

particles are entrapped by the ice front in the first frozen zone. During sintering, the necks formed by the entrapped particles would favor the atomic transport and form a dense layer at the bottom of the samples, as shown in Fig. 4b and c. Fig. 4 also reveals that the thickness of the dense layer increases as increasing the PAM content. It is due to the increase of the attractive force for the sample with increased PAM amount. With increasing PAM content from 1 to 2 wt.%, a longer distance is needed for decreasing the freezing velocity to a steady state where $F_\sigma \geq F_\eta$, and thus resulting in the increase in the thickness of the dense layer.

The influences of PAM additions on the α- to β-Si_3N_4 transformation and porosity of the investigated porous composites are shown in Table 1. It is clear that increasing the PAM content obviously reduces the amount of α- to β-Si_3N_4 transformation and slightly increases the porosity of the obtained samples. It is accepted that the densification and the growth of β-Si_3N_4 grains in Si_3N_4-based ceramics is generally via a liquid phase, through the process of solution–diffusion–reprecipitation. For the samples with PAM, during the growth of the ice crystals, Si_3N_4 particles together with PAM were expelled from the freezing front. During sintering, the removal of PAM would leave pores on porous Si_3N_4 walls, and thus retard the formation of necks among particles and impede atomic transport for α- to β-Si_3N_4 transformation by solution–diffusion–precipitation process. The typical microstructures of the obtained porous composites prepared with different PAM content are shown in Fig. 5. The aspect ratio of β-Si_3N_4 grains decreases obviously with increasing the PAM content, indicating that the incorporation of PAM inhibits the anisotropic growth of β-Si_3N_4 grains. It may be attributed to their different pore structures. In this study, the obtained composites are highly porous, so vapor phase transport cannot be discounted as a contribution to anisotropic β-Si_3N_4 growth [21]. As stated above, although the incorporation of PAM has no great influence on the porosity of the resultant materials, but significantly changed their pore structures, as shown in Fig. 1. For the material without PAM addition, although the porosity is slightly lower than that of the materials with PAM, the porosity is highly interconnected with dendritic pores, which would favor the anisotropic β-Si_3N_4 grain growth through vapor phase transport. In contrast, the addition of PAM obviously changes the pore structure from the lamellar pores with dendrites to columnar ones without dendritic pores, and thus resulting in the hindrance of β-Si_3N_4 grain growth due to the reduction in vapor phase transport.

The flexural strength and fracture toughness of the porous Si_3N_4 are shown in Table 1. It reveals that the mechanical properties of obtained porous composites are strongly affected by the microstructure, including pore structure and the morphology of β-Si_3N_4 grains. Lamellar pores with dentrites in the sample are easy to cause the damage of the obtained porous ceramics. Elongated β-Si_3N_4 grains and suitable interfacial bonding strength would improve the mechanical properties of the samples. As shown in Table 1, the sample with no PAM shows the lowest flexural strength and fracture toughness, although it possesses the highest β-Si_3N_4 content of 77.3% and more elongated microstructure. It may be attributed to its pore character, i.e., lamellar pores with obvious dendrites (Fig. 1a and b). The lamellar pores are easier to be torn than the columnar ones. Additionally, the main lamellar channels are interconnected by the dendritic pores, so the rapture might occur along dendritic pores and decrease the mechanical properties. In contrast, the sample with 2 wt.%PAM exhibits increased strength and toughness, although both β-Si_3N_4 content (38.9%) and the aspect ratio of β-Si_3N_4 grains are much lower than that of the sample without PAM. It is undoubtedly due to its different pore structure (columnar pores without dendrites, as shown in Fig. 1e and f). The sample with 1 wt.%PAM exhibits the highest strength and toughness in the resultant porous materials. It is attributed to its columnar pore structure with less dendritic pores and higher aspect ratio of β-Si_3N_4 grains.

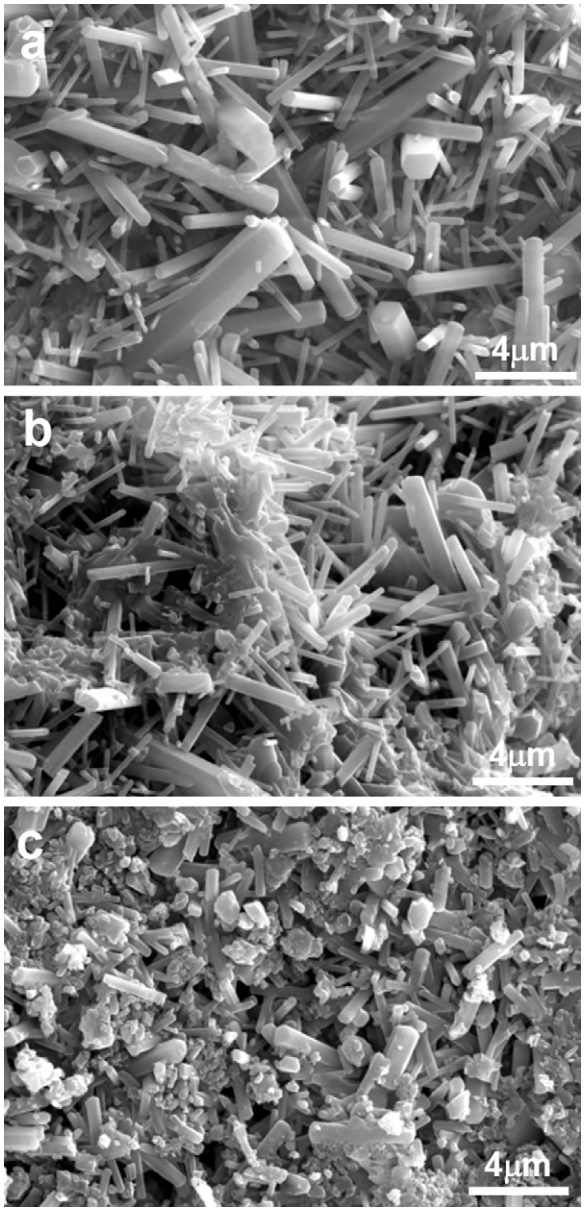

Fig. 5. SEM microstructure of the obtained porous Si_3N_4 ceramics with different PAM contents: (a) 0 wt.%PAM; (b) 1 wt.%PAM; (c) 2 wt.%PAM.

4. Summary

Porous BAS/Si_3N_4 composites with unidirectional aligned channels were fabricated by freeze casting using liquid N_2 as refrigerant. The incorporation of PAM has strong influence on the pore structure, morphology of β-Si_3N_4 grains and mechanical properties of the obtained porous β-Si_3N_4 composites. Increasing PAM content in the slurries changed the pore structure from lamellar pores with dendrites to columnar ones without dendrites, decreased the pore size and increased the dense layer thickness. The lamellar pores with dendrites could favor the $\alpha \rightarrow \beta$-Si_3N_4 transformation, but were detrimental to the mechanical properties. The composite with 1 wt.%PAM possesses the highest strength and toughness in the obtained porous composites. It is attributed to its columnar pore structure with less dendritic pores and higher aspect ratio of β-Si_3N_4 grains.

Acknowledgment

This work was supported by National Natural Science Foundation of China (Grant Nos. 90716022 and 50632020).

References

[1] U. Soltmann, H. Böttcher, D. Koch, G. Grathwohl, Mater. Lett. 57 (2003) 2861–2865.
[2] J.S. Lee, S.H. Lee, S.C. Choi, J. Alloys Compd. 467 (2009) 543–549.
[3] F.F. Lange, Int. Metal. Rev. 1 (1980) 1–20.
[4] M.J. Hoffmann, Mater. Res. Bull. 10 (1995) 28–32.
[5] A. Diaz, S. Hampshire, J. Eur. Ceram. Soc. 24 (2004) 413–419.
[6] J.F. Yang, Z.Y. Deng, T. Ohji, J. Eur. Ceram. Soc. 23 (2003) 371–378.
[7] C. Kawai, A. Yamakawa, J. Am. Ceram. Soc. 80 (1997) 2705–2708.
[8] J.F. Yang, G.J. Zhang, T. Ohji, J. Mater. Res. 16 (2001) 1916–1918.
[9] K. Ishizaki, S. Komarneni, M. Nanko, Porous Materials—Process Technology and Applications, Kluwer Academic Publishers, Norwell, 1998, pp. 1–11.
[10] T. Yokota, Chem. Eng. Jpn. 42 (1997) 845–851.
[11] T. Fukasawa, Z.-Y. Deng, M. Ando, T. Ohji, Y. Goto, J. Mater. Sci. 36 (2001) 2523–2527.
[12] S. Deville, E. Saiz, A.P. Tomsia, Acta Mater. 55 (2007) 1965–1974.
[13] L. Ren, Y.P. Zeng, D. Jiang, J. Am. Ceram. Soc. 90 (2007) 3001–3004.
[14] F. Ye, L.M. Liu, H.J. Zhang, B.S. Wen, J. Alloys Compd. 493 (2010) 272–275.
[15] F. Ye, J.C. Gu, Y. Zhou, M. Iwasa, J. Eur. Ceram. Soc. 23 (2003) 2203–2209.
[16] S.W. Quander, A. Bandyopadhyay, P.B. Aswath, J. Mater. Sci. 32 (1997) 2021–2029.
[17] G. Lipp, C. Körber, G. Rau, J. Cryst. Growth 99 (1990) 206–210.
[18] G.F. Bolling, J. Cissé, J. Cryst. Growth 10 (1971) 56–66.
[19] D.R. Uhlmann, B. Chalmers, K.A. Jackson, J. Appl. Phys. 35 (1964) 2986–2993.
[20] V.F. Petrenko, R.W. Whitworth, Physics of Ice, Oxford University Press, 2002.
[21] C. Kawai, A. Yamakawa, Ceram. Int. 24 (1998) 135–138.